sustainability

MDPI

Article

Parameters Identification of Photovoltaic Cell and Module Models Using Modified Social Group Optimization Algorithm

Habib Kraiem [1,2,*], Ezzeddine Touti [1,3,*], Abdulaziz Alanazi [1], Ahmed M. Agwa [1,4], Tarek I. Alanazi [5], Mohamed Jamli [3] and Lassaad Sbita [2]

1 Department of Electrical Engineering, College of Engineering, Northern Border University, Arar 73222, Saudi Arabia
2 Processes, Energy, Environment and Electrical Systems, National Engineering School of Gabes, University of Gabes, Gabes 6029, Tunisia
3 Laboratory of Industrial Systems and Renewable Energies, National Higher Engineering School of Tunis, Tunis 1008, Tunisia
4 Department of Electrical Engineering, Faculty of Engineering, Al-Azhar University, Cairo 11651, Egypt
5 Department of Physics, College of Science, Northern Border University, Arar 73222, Saudi Arabia
* Correspondence: alhabeeb.kareem@nbu.edu.sa (H.K.); esseddine.touti@nbu.edu.sa (E.T.)

Abstract: Photovoltaic systems have become more attractive alternatives to be integrated into electrical power systems. Therefore, PV cells have gained immense interest in studies related to their operation. A photovoltaic module's performance can be optimized by identifying the parameters of a photovoltaic cell to understand its behavior and simulate its characteristics from a given mathematical model. This work aims to extract and identify the parameters of photovoltaic cells using a novel metaheuristic algorithm named Modified Social Group Optimization (MSGO). First, a comparative study was carried out based on various technologies and models of photovoltaic modules. Then, the proposed MSGO algorithm was tested on a monocrystalline type of panel with its single-diode and double-diode models. Then, it was tested on an amorphous type of photovoltaic cell (hydrogenated amorphous silicon (a-Si: H)). Finally, an experimental validation was carried out to test the proposed MSGO algorithm and identify the parameters of the polycrystalline type of panel. All obtained results were compared to previous research findings. The present study showed that the MSGO is highly competitive and demonstrates better efficiency in parameter identification compared to other optimization algorithms. The Individual Absolute Error (IAE) obtained by the MSGO is better than the other errors for most measurement values in the case of single- and double-diode models. Relatedly, the average fitness function obtained by the MSGO algorithm has the fastest convergence rate.

Keywords: photovoltaic cells; modeling; parameters estimation; MSGO algorithm; optimization

Citation: Kraiem, H.; Touti, E.; Alanazi, A.; Agwa, A.M.; Alanazi, T.I.; Jamli, M.; Sbita, L. Parameters Identification of Photovoltaic Cell and Module Models Using Modified Social Group Optimization Algorithm. *Sustainability* **2023**, *15*, 10510. https://doi.org/10.3390/su151310510

Academic Editor: Mohamed A. Mohamed

Received: 9 May 2023
Revised: 17 June 2023
Accepted: 21 June 2023
Published: 4 July 2023

1. Introduction

In recent decades, due to their inexhaustibility, non-polluting nature, and highly adaptable properties to decentralized generation, renewable energies have been the ecological alternative to fossil fuels and nuclear energy [1,2]. For these reasons, advanced technologies are currently being developed to benefit from these types of energy sources. Photovoltaic (PV) panels, which generate electricity using the sun's energy as a renewable energy source, are one of the most prevalent forms of renewable energy [3]. Solar energy is growing exponentially. Its main characteristic is to be a form of decentralized production, making it possible to meet strong demand from citizens and local authorities and to produce energy where it is consumed. Consequently, significant losses can be avoided during energy transportation. The PV industry has been overgrowing in recent years [4] because it is not only inexhaustible but also silent and non-disturbing for residents, unlike wind turbines which cause visual and acoustic disturbances. In addition, the market to produce electricity from solar energy is proliferating [5,6]. In this context, the importance of photovoltaic generators connected to the electricity distribution network is growing rapidly [7]. Hence, assessing and studying the performance of the photovoltaic module, which is the fundamental component of these generators, appears to be highly significant [8]. The manufacturers typically tend to provide only limited operational data for PV panels. These data are only available under standard conditions of 1000 W/m^2 irradiation, 25 °C cell temperature, and air mass of 1.5 [9]. Therefore, it is essential to understand each cell element's physical properties and electrical characteristics before developing an equivalent circuit for a photovoltaic cell. Performance evaluation of PV modules and the design of energy systems are derived from the electrical characteristic current–voltage (I–V) of the modules under different radiation levels and different temperatures of the PV cell [10,11]. There are three forms of solar cell technologies available on the market: amorphous, monocrystalline, and polycrystalline [12]. Monocrystalline and polycrystalline cells are found in rigid panels. The difference between the two types is mainly based on their efficiency. To achieve maximum performance, crystalline panels should be installed perpendicular to the sun's rays. Generally abbreviated a-Si, amorphous silicon is the non-crystallized allotropic variety of silicon; crystalline structures of the a-Si are formed from disordered atoms that are not arranged regularly. Thin layers of amorphous silicon can be deposited at low temperatures on a wide variety of substrates. Hence, a wide range of microelectronic applications can be envisaged. The advantage of amorphous silicon cells is that they are environmentally friendly because they do not use toxic heavy metals, such as cadmium or lead. Compared to amorphous cells, crystalline panels do not perform as well in partial shadowing, and they lose a tiny percentage of their output as the temperature rises over 25 °C. Various equations can be used to model PV cells and modules approximated to differing degrees of accuracy from the actual device. This modeling offers essential advantages, such as ease of use, thanks to the equivalent electrical circuit and the popularization of the system properties. Therefore, the understanding of complex phenomena will be facilitated. Therefore, solar cells are considered power generators and will be modeled by equivalent circuits and electric models. The most commonly used are the single-diode model [13], the model with two diodes [14], and the one with three diodes [15]. Each of these models has some unknown parameters that characterize and describe the behavior of a PV generator. In addition, the behavior of PV generators is influenced by various parameters related to electrical modeling [16]. The power output of a photovoltaic (PV) cell is influenced by several factors such as the orientation of the panels, quality factor, kind of material, absorbent layer, and optical window. The optimal orientation of panels should be perpendicular to the sun's direction to maximize the power output. The quality factor of the cell is a measure of its efficiency to convert sunlight into electricity, and it involves a trade-off between efficiency and cost. The choices of material and the thickness and composition of the absorbent layer also play a significant role in determining the power output. Additionally, optimizing the optical window requires a balance between light transmission and absorption by the window. The PV cell's performance is interdependent on various parameters, such as efficiency, open-circuit voltage, fill factor, short-circuit current, and maximum power point. These parameters are interdependent, and there are constraints between them that must be considered to optimize the cell's performance. Hence, understanding the constraints between the PV cell parameters is vital for designing efficient PV systems.

In order to optimize the various characteristics and simulate the behavior of a PV generator, it is crucial to identify the physical mechanisms at play within it. The complexity of the model is determined by the number of parameters that need to be identified. The ideal model includes a current source for solar power input and a diode for the PN junction, but additional components can be added to better represent the PV cell's behavior in specific operational situations. Various methods of parameter identification have been studied in the literature, including numerical, analytical, deterministic, and metaheuristic methods. Numerical methods utilize mathematical algorithms to iteratively optimize parameter values using measured or simulated data. These methods employ numerical optimization techniques, including iterative algorithms and metaheuristic approaches, to minimize the discrepancy between model predictions and observed data. Numerical methods offer flexibility in handling complex and nonlinear problems [17,18]. Analytical methods involve analyzing mathematical formulas to identify the parameters of PV models. These methods are characterized by their short execution time and simplicity. However, their solutions are not precise [19,20]. The deterministic methods have major drawbacks, such as the high sensitivity to the initial hypotheses and the tendency of these algorithms to converge to the local optimum [21]. Moreover, they depend on the convexity of the model [22]. However, the models of photovoltaic cells are multimodal and characterized by nonlinearities. Recently, metaheuristic methods seem to be good potential alternatives for extracting parameters from PV models [23]. Indeed, they overcome the shortcomings of the analytical and deterministic methods already cited. In the following, we mention some of the most popular metaheuristic methods: Genetic Algorithm (GA) [24], artificial bee colony algorithm (ABC) [25], differential evolution algorithm (DE) [26], bird mating optimization (BMO) [27], Ant Lion Optimizer (ALO) [28], bacterial foraging optimization (BFO) [29], gray wolf optimization (GWO) [30], whale optimization algorithm (WOA) [31], Slime Mould Algorithm (SMA) [32], Sal Swarm Algorithm (SSA) [33], and Coyote Optimization Algorithm (COA) [15].

The primary objective of this study is to investigate and analyze the efficiency of a novel algorithm called Modified Social Group Optimization (MSGO) [34] for the extraction and identification of the parameters of photovoltaic cells. To provide a comprehensive assessment, a comparative study was conducted, incorporating various technologies and models of photovoltaic panel cells.

In the initial phase of this investigation, the proposed algorithm was applied to the monocrystalline photovoltaic panel of RTC France Company, considering both single- and double-diode cell models. The outcomes obtained through the MSGO algorithm were compared with results from previous studies utilizing alternative metaheuristic algorithms, such as the Nelder–Mead method and modified particle swarm optimization (NM–MPSO) [35], Levenberg–Marquardt algorithm combined with Simulated Annealing (LMSA) [36], ABC [21], biogeography-based optimization algorithm with mutation strategies (BBO-M) [37], improved adaptive differential evolution (Rcr-IJADE) [38], artificial bee swarm optimization algorithm (ABSO) [39], and chaotic asexual reproduction optimization (CARO) [40]. All these algorithms were tested on the same photovoltaic panel, under identical lighting and temperature conditions (temperature of 33 °C and irradiation of 1000 W/m^2).

Subsequently, the proposed algorithm was also evaluated on a flexible photovoltaic panel composed of hydrogenated amorphous silicon (a-Si: H). The obtained results were compared with the findings presented by authors from [41], who based their research on the optimization algorithms Quasi-Newton Method (QNM) and the Self-Organizing Migrating Algorithm (SOMA).

To validate the results obtained by the proposed MSGO algorithm, an experimental study was performed on the TITAN-12-50 panel, utilizing polycrystalline cells [42]. Finally, the paper concludes with a comparative analysis between different optimization algorithms employed for photovoltaic parameter extraction. The results obtained through the proposed MSGO algorithm are compared with those derived from other algorithms such as the WOA, SSA, Sine Cosine Algorithm (SCA), Virus Colony Search Algorithm (VCS), Gravitational Search Algorithm (GSA), and Ant Lion Optimizer (ALO). Throughout the remainder of this paper, three sections are described: Section 2 introduces PV models and problem formulation. Section 3 details the proposed MSGO algorithm. Section 4 treats the study of the MSGO algorithm efficiency by testing various pieces of technology and PV cell models. In the last section, the obtained results are compared with those given in previous studies.

2. Mathematical PV Model Analysis

The evaluation of the PV module performance and the power system design is based on the current–voltage electrical characteristic of the modules under different radiation levels and various temperatures of the PV cells. It is possible to model PV cells and modules by means of equations that approximate the physical cell to varying degrees. Several electrical models are proposed in the literature for simulating PV cells under different conditions. The model's complexity varies depending on the number of parameters (R_s, R_{sh}, etc.) to be considered. Every model is basically refinements of the ideal model, which consists of a diode that represents the PN junction and a current source that represents incident solar power.

It is possible to add several additional elements to provide a better representation of the behavior of PV cells in some operating areas [43]. Single-diode models (SDMs), double-diode models (DDMs), and three-diode models (TDMs) are the most used models. Figure 1a represents the single-diode model, which is regarded as the most popular model. It is widely used because of its simplicity. It also provides high precision and simplicity in the power generation quadrant.

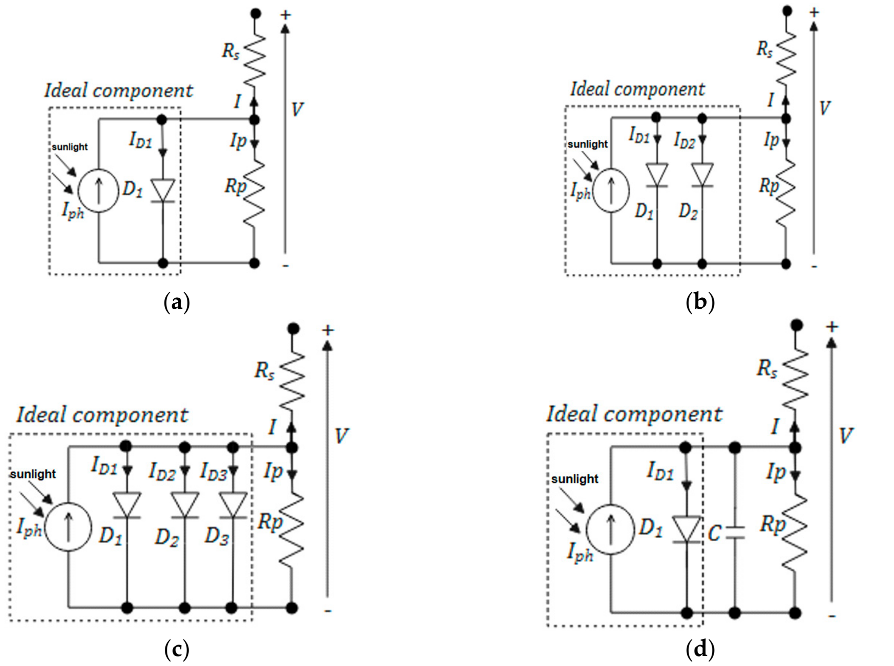

Figure 1. Solar cell models: (**a**) SDM, (**b**) DDM, (**c**) TDM, and (**d**) Dynamic Model.

The single-diode model has undergone various advancements that have led to the development of more accurate models, such as the Bishop model, which explains the behavior of the PV cell under reverse polarization. The double-diode model, shown in Figure 1b, considers losses due to various resistances and devices in the different electric components that constitute the circuit [44]. An enhanced model considers the effects of grain boundaries and leakage currents. This model involves three diodes as it is shown in Figure 1c. Although this model meets most of the physical requirements of solar cells, it involves computing nine parameters that require exceptionally high numerical execution. In addition, dynamic models are proposed by introducing the capacity to model the dynamic behavior of the PV cell. This model type is shown in Figure 1d. All these models differ in the number of parameters required for computing the I–V characteristic [45].

I_{ph} is the photo-generated current source; I_{D1}, I_{D2}, I_{D3} are the currents of diodes D_1, D_2, and D_3; R_p is the shunt resistance; R_s is the series resistance; I is the output current; and V is the output voltage.

2.1. Mathematical Development

2.1.1. Crystalline Cells

From the equivalent circuit (Figure 1a), it is evident that the current produced by the solar cell is equal to that produced by the current source (I_{ph}), minus that which flows through the diode (I_d), minus that which flows through the shunt resistor (I_p).

$$I = I_{ph} - K_i I_d - I_p \tag{1}$$

where $K_i = \begin{cases} K_1 = \begin{bmatrix} 1 & 0 & 0 \end{bmatrix},\ i = 1 \text{ in case of SDM} \\ K_2 = \begin{bmatrix} 1 & 1 & 0 \end{bmatrix},\ i = 2 \text{ in case of DDM} \\ K_3 = \begin{bmatrix} 1 & 1 & 1 \end{bmatrix},\ i = 3 \text{ in case of TDM} \end{cases}$, where $I_d = \begin{bmatrix} I_{d1} \\ I_{d2} \\ I_{d3} \end{bmatrix}$, and $I_p = \frac{V+R_sI}{R_p}$.

The current in the j^{th} diode is given by

$$I_{dj} = I_{sdj}\left(e^{\left(\frac{q(V+R_sI)}{n_jKT}\right)} - 1\right),\ (j = 1, 2, 3) \tag{2}$$

Then, the current given in Equation (1) is given by Equation (3), where I_{SDM}, I_{DDM}, and I_{TDM} are the total output current when considering the SDM, DDM, and TDM, respectively.

$$\begin{cases} I_{SDM} = I_{ph} - I_{sd}\left(e^{\left(\frac{q(V+R_sI)}{n_1KT}\right)} - 1\right) - \frac{V+R_sI}{R_p} \\ I_{DDM} = I_{ph} - I_{sd1}\left[e^{\frac{q(V+R_sI)}{n_1KT}} - 1\right] - I_{sd2}\left[e^{\frac{q(V+R_sI)}{n_2KT}} - 1\right] - \frac{V+R_sI}{R_p} \\ I_{TDM} = I_{ph} - I_{sd1}\left[e^{\frac{q(V+R_sI)}{n_1KT}} - 1\right] - I_{sd2}\left[e^{\frac{q(V+R_sI)}{n_2KT}} - 1\right] - I_{sd3}\left[e^{\frac{q(V+R_sI)}{n_3KT}} - 1\right] - \frac{V+R_sI}{R_p} \end{cases} \tag{3}$$

where n_1, n_2, and n_3 are the ideality factors of the diodes D_1, D_2, and D_3; K is the Boltzmann constant (1.380649×10^{-23} Joule/Kelvin); T is the temperature of the PV panel (Kelvin); and q is the charge of the electron ($1.602176634 \times 10^{-19}$ Coulomb).

The TDM does not seem suitable for fast computations and has complex nonlinear analytic expressions; therefore, this model will be excluded from the parametric identification tests.

2.1.2. Amorphous Silicon Cell

Equation (4) defines the current–voltage characteristic for an amorphous silicon cell:

$$I = I_{ph}\left(1 - \frac{d_i^2}{\mu_{eff}[V_b - (V + IR_s)]}\right) - I_s\left[\exp\left(\frac{V + IR_s}{aV_T} - 1\right)\right] - \frac{V + IR_s}{R_{sh}} \tag{4}$$

d_i denotes the width of the i^{th} layer in the (a-Si) p_i_n diode, μ_{eff} represents the mobility-lifetime product of the electron and hole, and V_{bi} is the built-in field voltage.

The diode reverse saturation current and the photo-generated current of an (a-Si) cell under constant light and temperature are given, respectively, by

$$I_{ph} = qAg(x)\left(L_p + L_n + W\right) \tag{5}$$

$$I_0 = J_s \times A = \left(\frac{qD_p p_{n0}}{L_p} + \frac{qD_n n_{p0}}{L_n}\right) \times A \tag{6}$$

where A is the p_n junction area, L_p is the carrier diffusion length of the p-type area, L_n is the carrier diffusion length of the n-type area, W is the depletion layer, D_p and D_n are the holes and electrons diffusion coefficient, p_{n0} and n_{p0} are the minority carrier concentration in the P region and N region, and $g(x)$ is the electron hole formation ratio.

2.2. The Objective Functions

The term objective function is used in mathematical optimization and operations research to refer to a function that acts as a criterion for identifying the best solution to an optimization problem.

The objective function of the SDM may be written as

$$f_{SDM}(V,\ I,\ X) = I - X(1) + X(2)\left[e^{\left(\frac{q(V+X(3)I)}{X(4)KT}\right)} - 1\right] + \frac{V + X(3)I}{X(5)} \tag{7}$$

$$X = \begin{bmatrix} I_{ph} & I_{sd} & R_s & n_1 & R_p \end{bmatrix}$$

For the DDM, the error function is expressed by

$$f_{DDM}(V, I, X) = I - X(1) + X(2)\left[e^{\left(\frac{q(V+X(3)I)}{X(4)KT}\right)} - 1\right] + X(5)\left[e^{\left(\frac{q(V+X(3)I)}{X(6)KT}\right)} - 1\right] + \frac{V + X(3)I}{X(7)} \tag{8}$$

where $X = \begin{bmatrix} I_{ph} & I_{sd_1} & R_s & n_1 & I_{sd_2} & n_2 & R_p \end{bmatrix}$.

Whereas, the error function for the TDM is defined by

$$\begin{aligned} f_{TDM}(V, I, X) = I - X(1) + X(2)\left[e^{\left(\frac{q(V+X(3)I)}{X(4)KT}\right)} - 1\right] + X(5)\left[e^{\left(\frac{q(V+X(3)I)}{X(6)KT}\right)} - 1\right] \\ +X(7)\left[e^{\left(\frac{q(V+X(3)I)}{X(8)KT}\right)} - 1\right] + \frac{V+X(3)I}{X(9)} \end{aligned} \tag{9}$$

where $X = \begin{bmatrix} I_{ph} & I_{sd_1} & R_s & n_1 & I_{sd_2} & n_2 & I_{sd_3} & n_3 & R_p \end{bmatrix}$.

It is necessary to use *Ne* samples (data points number) to widen the scope of the search and reach the global optimum. Equation (10) gives us a description of the cost function:

$$\mathrm{RMSE}(x) = \sqrt{\frac{1}{Ne}\sum_{C=1}^{Ne}\left(f_M^C(V^C, I^C, x)\right)^2} \tag{10}$$

3. Procedure of Social Group Optimization for PV Parameters Estimation

The past twenty years have seen a remarkable rise in interest in metaheuristic optimization algorithms. The research work developed has enabled the appearance of new algorithms which are generally based on the following:

- A new idea inspired by a natural, physical, chemical phenomena;
- A modification of an existing algorithm to improve its performances;
- The hybridization of two methods allows the strengths to merge and the weaknesses to be eliminated of the two algorithms.

However, no algorithm can be adapted to all types of problems. In 2016, a new metaheuristic optimization algorithm appeared, known as Social Group Optimization (SGO) [46]. To solve complex problems, the new algorithm was inspired by the social behavior of individuals in groups. Each individual's knowledge is mapped by its fitness. The algorithm contains two phases. The first phase is called the improving phase in which each individual interacts with the best person (best solution) to improve his knowledge by interacting. The second phase is named the acquiring phase, during which the individuals acquire knowledge when they interact with the best person and randomly selected individuals simultaneously. A comparative study is carried out to show the performance of the new method. Detailed information on the SGO algorithm can be found in the following articles [47,48]. The SGO algorithm is described with the following:

P_i, (i = 1, 2, 3, ..., N): Pi is the social group persons, and N is the total number of people in the social group.

P_{ij}, (j = 1, 2, ..., D): D is the traits number related to a person which allows us to determine the dimensions of a person.

f_i, (i = 1, 2, ..., N) is their corresponding fitness value.

Improving phase

In each social group, the role of the best person (P_{best}) is to propagate knowledge between all persons. As a result, others in the group enhance their knowledge.

$$[minvalue, index] = \min\{f(Pi),\ i = 1,2,3\ldots\ldots\ldots.N\}$$

$$\text{gbest} = \text{P}(\text{index}, :)$$

The following algorithm (Algorithm 1) can be used to calculate how often each person's knowledge is updated:

Algorithm 1 Improving phase

for i = 1: *N*
  for j = 1: *D*
    $Pnew_{ij}$ = *c* * *Pij* + *r* * (*Pbest*(*j*) − *Pij*)
  end for
end for

r: random number, and $r \in [0, 1]$. If *Pnew* provides higher fitness than P_{old}, it is accepted [34]. *c* is the parameter of self-introspection $c \in [0, 1]$.

Acquiring Phase

In the acquiring phase (Algorithm 2), a person acquires new knowledge by interacting with other persons of the group. The interaction can be with the best person (*Pbest*) or randomly with other persons who have more knowledge. To acquire knowledge, a person always interacts with the *Pbest* and with any other person of the group who has more knowledge than him. The ability to obtain a quantity of knowledge from another person is defined by the self-awareness probability (SAP). The modified acquiring phase is computed as

$$[value,\ index\_num] = \min\{f(Pi),\ i = 1,2,3,\ 4\ldots\ldots\ldots.N\}$$

$$Pbest = P(index\_num, :)$$

where *Pi* is the updated value at the completion of the improving phase.

Algorithm 2 Acquiring phase

for i = 1: *N*
  Randomly select one person P_r *where* $i \neq r$
    If $f(P_i) < f(P_r)$
      If rand > *SAP*
        for j = 1: *D*
        $Pnew_{i,j} = P_{i,j} + rand_1 * (P_{i,j} - P_{r,j}) + rand_2 * (best_p\ (j) - P_{i,j})$
      end for
  else
        for j = 1: *D*
        $Pnew_{i,j} = lb + rand_2 * (ub - lb)$
        end for
      end if
  else
      for j = 1: *D*
      $Pnew_{i,j} = P_{i,j} + rand_1 * (P_{r,j} - P_{r,j}) + rand_2 * (best_p\ (j) - P_{i,j})$
      end for
  end if
end for

Pnew is accepted if it provides a higher level of fitness than *P*.

The general steps to use the MSGO algorithm to extract parameters of a PV cell include:

Step 1: Define the objective function which describes the behavior of the PV cell under different conditions. This function takes input parameters, such as the cell's temperature, irradiance, and voltage, and outputs a value that represents the cell's performance. The goal is to find the values of these input parameters that maximize the output value of the objective function.

Step 2: Define the parameter space. The parameter space defines the objective function constraints for each parameter, such as the temperature may range from −10 °C to 100 °C, the irradiance may range from 0 W/m^2 to 1000 W/m^2, and the voltage may range from 0 V to 1 V. All other range parameters are declared in Equations (15)–(17).

Step 3: Initialize the population. The population (P_i) is a set of solutions that are randomly generated within the parameter space. Each solution corresponds to a set of input parameters that are used to evaluate the objective function.

Step 4: Evaluate the fitness. The fitness is a measure of how well each solution performs with respect to the objective function. The fitness function takes as input the output value of the objective function and returns a scalar value that represents the quality of the solution. The higher the fitness, the better the solution.

Step 5: Update the population. The MSGO algorithm updates the population in two phases: the improving phase and the acquiring phase. In the improving phase, each individual interacts with the best person in the social group to improve its knowledge. In the acquiring phase, each individual acquires knowledge by interacting with the best person and randomly selected individuals. The updating of each person's knowledge can be calculated using the formula described in the improving phase.

Step 6: Repeat steps 4 and 5 until convergence. The optimization process continues until the fitness values converge to a satisfactory level or the maximum number of iterations is reached. The best solution found during the optimization process corresponds to the set of input parameters that maximizes the output value of the objective function. These parameters can be used to characterize the behavior of the PV cell under the given conditions.

4. Results

The technical details of the software and hardware used for the extraction of the various simulation results are given in Table 1.

Table 1. Software and hardware details.

Hardware and Software	Setting
CPU	Intel (R) Core (TM) i7—7500U
Frequency	2.9 GHz
RAM	12 Gb
Simulation software	Matlab R2018b
Operating System	Windows 10

The adjustable parameters of the MSGO algorithm include: the population size is 40, and the maximum number of iterations is 3000. However, the parameters of other comparative algorithms are given in references cited in the first section.

All simulation work was conducted under the following solar irradiance and temperature conditions: 1000 W/m^2 and 33 °C. The obtained results of our parameter identification algorithm were compared to other optimization algorithms to determine the accuracy of the fitted curve between the MSGO algorithm values and experimental data. Table 2 summarizes the comparison work established in this paper.

Table 2. Summary of comparative study.

Types of Tested Panels	PV Cell Model	Examined Algorithms during the Comparison
RTC France Company monocrystalline	Single diode	NM–MPSO, LMSA, ABC, BBO-M, Rcr-IJADE
	Double diode	NM–MPSO, Rcr-IJADE, ABSO, CARO, ABC
Hydrogenated Amorphous Silicon a-Si: H	Single diode	SOMA, QNM
TITAN-12-50 Polycrystalline	Double diode	SCA, ALO, GSA, VCS, WOA, SSA

4.1. MSGO Implementation

To verify the accuracy of the fitted curve obtained by the MSGO algorithm using experimental data, a comparison is made against other algorithms. Tables 3 and 4 present a statistical analysis of the contrasted results for each model. The statistical errors used to demonstrate the performance of the proposed algorithm are presented below.

Table 3. Extracted parameters in case of an SDM.

Algorithm	I_{ph} (A)	I_0 (µA)	n	R_s (Ω)	R_p (Ω)
MSGO	0.7607877	0.31058918	1.47725615	0.0365470	52.88998
BBO-M	0.760781	0.318743	1.479842	0.036422	53.36226
Rcr-IJADE	0.760775	0.323022	1.481183	0.036376	53.718525
LMSA	0.760781	0.318492	1.479764	0.036433	53.326441
CARO	0.760792	0.317243	1.481681	0.036443	53.08930
ABC	0.76082	0.325155	1.481731	0.036443	53.64332
NM–MPSO	0.760781	0.323065	1.481202	0.036384	53.72221

Table 4. The estimated data and the resulted IAE obtained by the proposed algorithm **MSGO** compared with other algorithms in the case of an SDM.

	V_{exp} (V)	I_{exp} (A)	I_{est} (A)	MSGO	R_{cr}-IJADE	BBO-M	ABC	LMSA	NM–MPSO
1	−0.2057	0.764	0.764149248	0.00014925	0.00009559	0.000006	0.0001	0.000115762	0.000087
2	−0.1291	0.762	0.762293808	0.00029381	0.00066611	0.000604	0.0006	0.000680672	0.000662
3	−0.0588	0.7605	0.761373566	0.00087357	0.00085473	0.000817	0.0008	0.000863281	0.000854
4	0.0057	0.7605	0.7601543024	0.00034570	0.00035034	0.000364	0.0003	0.000346856	0.000346
5	0.0646	0.76	0.759038854	0.00096115	0.00094298	0.000946	0.0009	0.000953669	0.000945
6	0.1185	0.759	0.758010563	0.00098944	0.00095528	0.000943	0.0009	0.000973813	0.000957
7	0.1678	0.757	0.757045517	0.00004552	0.00009510	0.000120	0.0001	0.0000690271	0.000091
8	0.2132	0.757	0.756084674	0.00091533	0.00084950	0.000817	0.0008	0.000886778	0.000858
9	0.2545	0.7555	0.755022264	0.00047774	0.00041823	0.000361	0.0004	0.000445307	0.000413
10	0.2924	0.754	0.753597432	0.00040257	0.00032967	0.000276	0.0003	0.000370139	0.000336
11	0.3269	0.7505	0.751327686	0.00082769	0.00089542	0.000953	0.0008	0.000858429	0.000888
12	0.3585	0.7465	0.747306479	0.00080648	0.00085737	0.000914	0.0008	0.000827345	0.000848
13	0.3873	0.7385	0.740087107	0.00158711	0.00160420	0.001668	0.0016	0.00160213	0.001596
14	0.4137	0.728	0.727430948	0.00056905	0.00059912	0.000583	0.0006	0.000616337	0.000604
15	0.4373	0.7065	0.707034237	0.00053424	0.00044631	0.000485	0.0004	0.000492923	0.000452
16	0.459	0.6755	0.675413782	0.00008622	0.00019600	0.000230	0.0002	0.000182486	0.000206
17	0.4784	0.632	0.631018287	0.00098171	0.00110900	0.001271	0.0012	0.001194906	0.001117
18	0.496	0.573	0.572202755	0.00079724	0.00091027	0.001112	0.0011	0.001026552	0.00092
19	0.5119	0.499	0.499575662	0.00057566	0.00049902	0.000563	0.0005	0.000638902	0.00049
20	0.5265	0.413	0.413530488	0.00053049	0.00049030	0.000612	0.0006	0.00065758	0.000492
21	0.5398	0.3165	0.31721586	0.00071586	0.00071532	0.000985	0.001	0.000992379	0.000718
22	0.5521	0.212	0.212079153	0.00007915	0.00010468	0.000142	0.0001	0.000112783	0.000102
23	0.5633	0.1035	0.102706638	0.00079336	0.00078397	0.001254	0.0012	0.001305993	0.000779
24	0.5736	−0.01	−0.009221842	0.00077816	0.00075437	0.001268	0.0013	0.001228583	0.000751
25	0.5833	−0.123	−0.12427906	0.00127906	0.00137750	0.002537	0.0024	0.002545248	0.001381
26	0.59	−0.21	−0.209015291	0.00098471	0.00080320	0.001469	0.0015	0.001522512	0.000807

- The Individual Absolute Error (IAE) is defined by

$$\text{IAE} = |I_{measured} - I_{estimated}| \tag{11}$$

- The Median Absolute Error (MAE) is expressed as

$$\text{MAE} = \sum_{i=1}^{m} \frac{|I_{measured} - I_{estimated}|}{m} \tag{12}$$

- The Residual Sum of Squares (SSE) is defined by

$$\text{SSE} = \sum_{i=1}^{N_e} (I_{measured} - I_{estimated})^2 \tag{13}$$

- The Root Mean Square Error (RMSE) is given by

$$\text{RMSE} = \sqrt{\frac{1}{N_e} \sum_{i=1}^{N_e} (I_{measured} - I_{estimated})^2} \tag{14}$$

The equations below present the objective function constraints for each model, both for single and double diodes. The objective function constraints for the SDM is given by

$$\begin{cases} 0 \le I_{ph} \le 1 \text{ A} \\ 0 \le I_{01} \le 1 \times 10^{-7} \text{ A} \\ 1 \le n_1 \le 2 \\ 0 \le R_s \le 0.8 \ \Omega \\ 0 \le R_p \le 100 \ \Omega \end{cases} \tag{15}$$

The objective function constraints for the DDM are

$$\begin{cases} 0 \le I_{ph} \le 1 \text{ A} \\ 0 \le I_{01} \le 1 \times 10^{-7} \text{A} \\ 0 \le I_{02} \le 1 \times 10^{-7} \text{A} \\ 1 \le n_1 \le 2 \\ 1 \le n_2 \le 2 \\ 0 \le R_s \le 0.5 \ \Omega \\ 0 \le R_p \le 100 \ \Omega \end{cases} \tag{16}$$

The objective function constraints for (a-Si: H) are

$$\begin{cases} 0 \le I_{ph} \le 1 \ \mu\text{A} \\ 0 \le d \le 10 \times 10^{-8} \text{ m} \\ 0 \le \mu_{eff} \le 10 \left(\text{cm}^2/V\right) \\ 0 \le V_{bi} \le 1.5 \text{ V} \\ 0 \le R_s \le 0.5 \ \Omega \\ 0 \le I_s \le 5 \times 10^{-14} \\ 1 \le a \le 2.5 \\ 0 \le R_{sh} \le 50 \ \Omega \end{cases} \tag{17}$$

4.1.1. A Comparative Study of Extraction Parameters for the SDM

The extracted parameters using the MSGO algorithm for the SDM are presented in Table 3. These values are compared to those obtained by other algorithms such as **BBO-M**, $\mathbf{R_{cr}}$**-IJADE**, **LMSA**, **CARO**, **ABC**, and **NM–MPSO**.

The estimated current values obtained by the proposed algorithm and the resulted IAE are given in Table 4. These results are compared to those obtained by the $\mathbf{R_{cr}}$**-IJADE,**

BBO-M, **ABC**, **LMSA**, and **NM–MPSO** algorithms. As it is shown, the IAE (IAT) obtained by the MSGO algorithm is better than the other errors for most measurement values.

The various statistical errors already defined by Equations (11)–(14) are presented in Table 5 and compared with those obtained by the other algorithms. One can remark that the MSGO error IAT (IAE) has the lowest value, which proves the robustness of the used algorithm.

Table 5. Statistical results for the SDM.

	MSGO	BBO-M	R_{cr}-IJADE	LMSA	CARO	ABC	NM–MPSO
IAT	0.01738	0.0213	0.017704	0.0215	0.0182	0.0205	0.0177
RMSE	7.21×10^{-4}	9.86×10^{-4}	7.75×10^{-4}	9.86×10^{-4}	9.87×10^{-4}	9.49×10^{-4}	7.75×10^{-4}
SSE	1.355×10^{-5}	2.529×10^{-5}	1.562×10^{-5}	2.529×10^{-5}	2.531×10^{-5}	2.343×10^{-5}	1.563×10^{-5}
MAE	6.68×10^{-4}	8.19×10^{-4}	6.81×10^{-4}	8.27×10^{-4}	6.98×10^{-4}	7.88×10^{-4}	6.81×10^{-4}

The different IAE results given in Table 4 are illustrated in Figure 2. One can notice that the IAE obtained by the MSGO algorithm (red color) is the lowest error for most values.

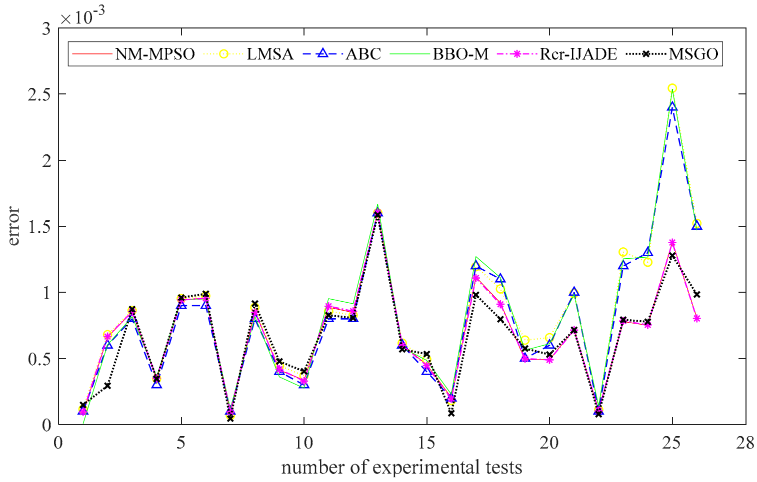

Figure 2. Calculated errors IAE obtained with the MSGO, R_{cr}-IJADE, BBO-M, ABC, LMSA, and NM–MPSO algorithms: case of SDM.

In order to assess the precision of the extracted parameters, one compares the I–V and P–V characteristics obtained from the estimated parameters using the MSGO method with the experimental data. Figure 3 illustrates this comparison, specifically for a single-diode case. These figures allow us to evaluate the quality of the parameter estimation process.

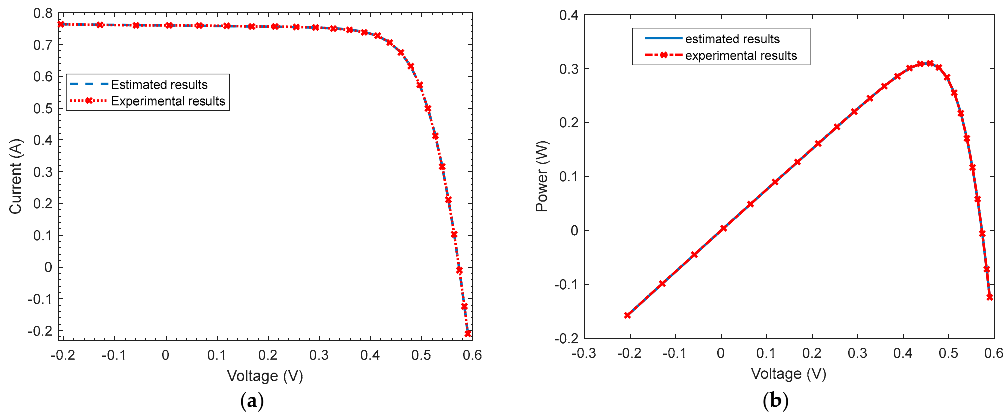

Figure 3. Experimental and estimated results obtained by the proposed **MSGO** algorithm in the case of an **SDM**: (**a**) Current_Voltage; (**b**) Power_Voltage.

The results depicted in Figure 3 indicate that the reconstructed SDM aligns well with the experimental data.

4.1.2. A Comparative Study of Extraction Parameters for the DDM

The extracted parameters using the MSGO algorithm for the DDM are presented in Table 6. These values are compared to those obtained by other algorithms, such as **BBO-M**, **R_{cr}-IJADE**, **LMSA**, **CARO**, **ABC**, and **NM–MPSO**.

Table 6. Extracted parameters in the case of double-diode model.

Algorithm	I_{ph} (A)	I_{01} (µA)	I_{02} (µA)	n_1	n_2	R_s (Ω)	R_p (Ω)
MSGO	0.7607	0.1465	0.6300	1.4190	1.8075	0.0371	54.7897
R_{cr}-IJADE	0.760821	0.225974	0.749347	1.451017	2.0000	0.036740	55.485443
CARO	0.760752	0.293151	0.090982	1.473383	1.77322	0.036414	54.39674
ABSO	0.760783	0.267135	0.381914	1.465125	1.98152	0.036572	54.62193
ABC	0.760825	0.040712	0.287433	1.449541	1.48852	0.036445	53.78046
NM–MPSO	0.760782	0.224761	0.755245	1.45054	1.99998	0.036752	55.52967

The estimated current values obtained by the proposed algorithm and the resulted IAE are given in Table 7. These results are compared to those obtained by the **R_{cr}-IJADE, BBO-M**, **ABC**, **LMSA**, and **NM–MPSO** algorithms. As it is shown, the IAE (IAT) obtained by the MSGO algorithm is better than the other errors for the majority of measurement values.

Table 7. Estimated data and the resulted IAE obtained by the proposed algorithm **MSGO** compared with other algorithms.

	V_{exp} (V)	I_{exp} (A)	I_{est} (A)	MSGO	ABC	CARO	ABSO	R_{cr}-IJADE	NM–MPSO
1	−0.2057	0.764	0.76402813	0.0000281297	0.000092908	0.00031	0.000031	0.00009268	0.000023
2	−0.1291	0.762	0.762630936	0.000630936	0.0006	0.000629	0.000629	0.00065394	0.000598
3	−0.0588	0.7605	0.761348408	0.000848408	0.0008	0.000843	0.000843	0.00085755	0.000832
4	0.0057	0.7605	0.760170729	0.000329271	0.0003	0.000338	0.000338	0.00033747	0.00033
5	0.0646	0.76	0.759091932	0.000908068	0.0009	0.00092	0.00092	0.00094	0.000895
6	0.1185	0.759	0.758093995	0.000906005	0.0009	0.000919	0.000919	0.00094935	0.00088
7	0.1678	0.757	0.757150045	0.000150045	0.0001	0.000139	0.000139	0.00009635	0.000187
8	0.2132	0.757	0.756196358	0.000803642	0.0008	0.000807	0.000807	0.00085535	0.000757
9	0.2545	0.7555	0.755121281	0.000378719	0.0004	0.000368	0.000368	0.00041885	0.000323
10	0.2924	0.754	0.753659367	0.000340633	0.0003	0.000306	0.000306	0.00033126	0.000277
11	0.3269	0.7505	0.751329108	0.000829108	0.0008	0.000892	0.000892	0.00089511	0.000896
12	0.3585	0.7465	0.74723368	0.00073368	0.0008	0.000822	0.000822	0.00084939	0.000798
13	0.3873	0.7385	0.739947501	0.001447501	0.0016	0.001544	0.001544	0.00160214	0.0001495
14	0.4137	0.728	0.727258182	0.000741818	0.0006	0.000669	0.000669	0.00061216	0.000729
15	0.4373	0.7065	0.706880574	0.000380574	0.0004	0.000396	0.000396	0.00045162	0.000344
16	0.459	0.6755	0.675327647	0.000172353	0.0002	0.000235	0.000235	0.00019888	0.000259
17	0.4784	0.632	0.631016281	0.000983719	0.0012	0.001111	0.001111	0.00111234	0.0001099
18	0.496	0.573	0.572261627	0.000738373	0.0011	0.000886	0.000886	0.00092523	0.000845
19	0.5119	0.499	0.499644454	0.000644454	0.0005	0.000533	0.000533	0.00049417	0.000586
20	0.5265	0.413	0.413556808	0.000556808	0.0006	0.000525	0.000525	0.00049125	0.000571
21	0.5398	0.3165	0.317169103	0.000669103	0.001	0.00073	0.00073	0.00071918	0.000753
22	0.5521	0.212	0.211959679	0.0000403211	0.0001	0.00009	0.00009	0.00010831	0.00088
23	0.5633	0.1035	0.102545511	0.000954489	0.0012	0.000806	0.000806	0.00077968	0.000827
24	0.5736	−0.01	−0.009374369	0.000625631	0.0012	0.00073	0.00073	0.00075539	0.000711
25	0.5833	−0.123	−0.124360342	0.001360342	0.0025	0.00139	0.00139	0.00137667	0.0001388
26	0.59	−0.21	−0.209001839	0.000998161	0.0014	0.00083	0.00083	0.00080501	0.000865

The various statistical errors already defined by Equations (11)–(14) are presented in Table 3 and compared with those obtained by the other algorithms. One can remark that the MSGO error IAT (IEA) has the lowest value, which proves the robustness of the used algorithm.

The various IAE results given in Table 7 are illustrated in Figure 4. One can notice that the IAE obtained by the MSGO algorithm (red color) is the lowest error for most values.

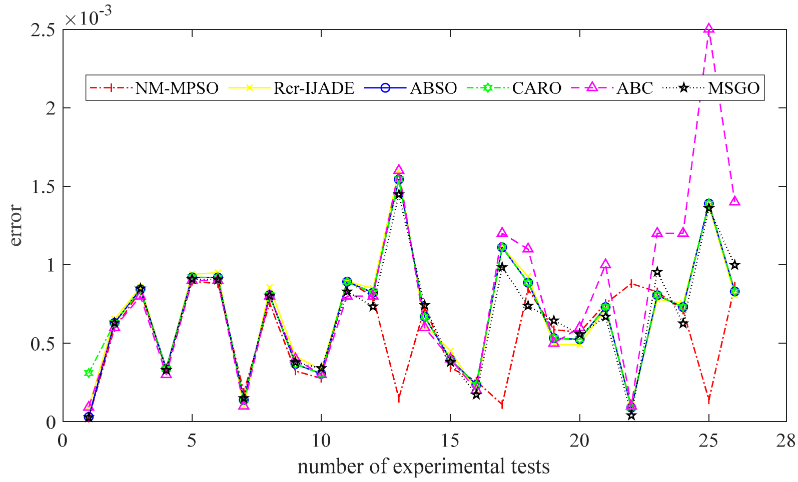

Figure 4. Calculated errors IAE obtained using the MSGO, ABC, CARO, ABSO, R_{cr}-IJADE, and NM–MPSO algorithms: case of DDM.

The I–V and P–V characteristics resulting from the parameters identified using the MSGO algorithm are compared to both experimental and estimated data to evaluate their quality. Figure 5 provides a comparison for a scenario involving two diodes, allowing us to determine the accuracy of the parameter estimation achieved through the MSGO algorithm. The results of the parameter identification using the MSGO algorithm and experimental data are compared with the estimated data to investigate the quality of the extracted parameters.

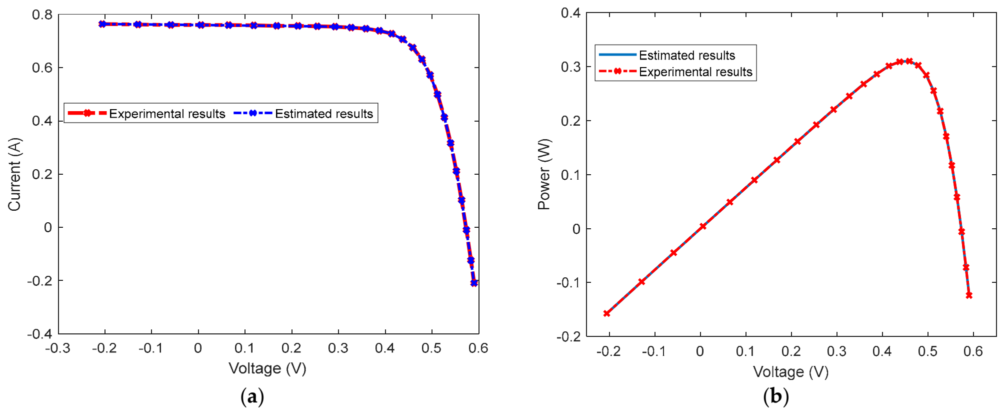

Figure 5. Experimental and estimated results obtained by the proposed MSGO algorithm in the case of a **DDM**: (**a**) Current_Voltage; (**b**) Power_Voltage.

Figure 6a,b illustrate the estimated I–V characteristic of the SDM and DDM compared with the experimental one. It is noted that there is a slight advantage of the DDM compared to the SDM, which is not clear enough in the figure. Upon closer inspection of the corresponding statistical results given in Tables 5 and 8, it becomes evident that the DDM outperforms the SDM by a small margin.

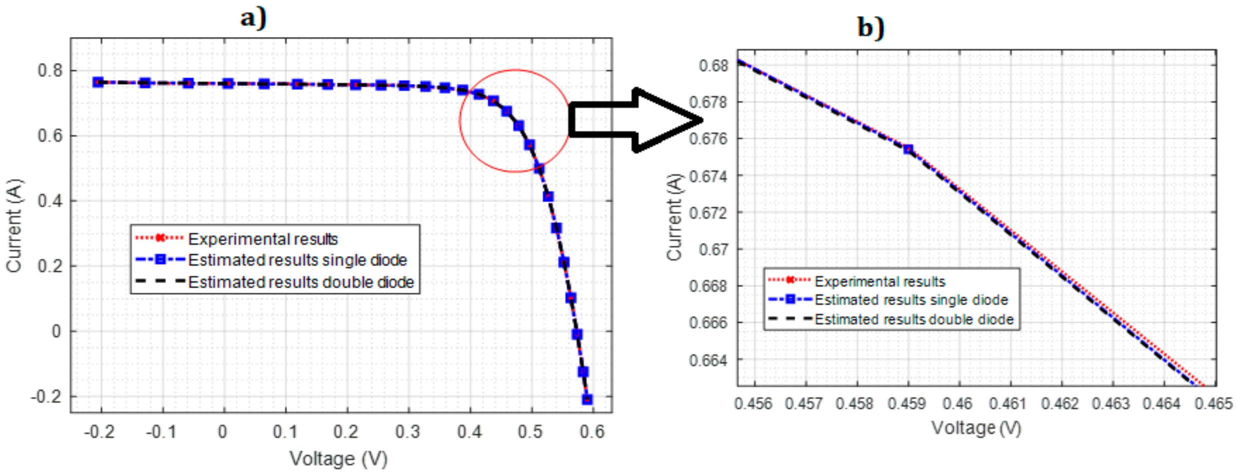

Figure 6. Experimental and estimated results: (**a**) I–V characteristic for SDM and DDM, and (**b**) Zoom of I–V characteristic in Figure 5a.

Table 8. Statistical results for the DDM (RTC France Company).

	MSGO	R_{cr}-IJADE	CARO	ABSO	ABC	NM–MPSO
Total IAE	0.0172	0.0177	0.0693	0.0178	0.0204	0.0174
RMSE	7.514×10^{-4}	7.754×10^{-4}	8.1×10^{-4}	7.682×10^{-4}	9.922×10^{-4}	7.581×10^{-4}
SSE	1.468×10^{-5}	1.56×10^{-5}	1.7×10^{-5}	1.53×10^{-5}	2.56×10^{-5}	1.49×10^{-5}
MAE	6.62×10^{-4}	6.81×10^{-4}	2.67×10^{-4}	6.83×10^{-4}	7.84×10^{-4}	6.68×10^{-4}

4.1.3. A Comparative Study of Extraction Parameters for the Amorphous PV Cell

The extracted parameters using the **MSGO** algorithm for the amorphous model are presented in Table 9. These values are compared to those obtained by other algorithms such as **QNM** and **SOMA**.

Table 9. Extracted parameters in case of amorphous cell.

Algorithm	I_{ph} (A)	d (10^{-8} m)	μ_{eff} (cm^2/V)	V_{bi} (V)	R_s (Ω)	I_s (A)	a	R_{sh} (Ω)
MSGO	0.3123	4.72	3.03	0.97	0.295	1.5	1.918	11.07
QNM	0.3043	5.8065	4.8812	0.9759	0.4242	3.0691	1.999	11.9138
SOMA	0.3181	4.9743	3.3277	0.9963	0.4706	3.0783	1.9931	13.9288

The various IAE results given by Table 10 are illustrated in Figure 7. One can notice that the IAE obtained by the MSGO algorithm (red color) is the lowest error for most values, as is confirmed in Table 11.

Table 10. Estimated data and resulted IAE obtained by the proposed algorithm **MSGO**.

	V_{exp} (V)	I_{exp} (A)	I_{est} (A)	IAE		
				MSGO	QNM	SOMA
1	1.525	0	−0.00328	0.00328	0.0041	0.00086
2	1.515	0.0158	0.0137831	0.002017	0.0058	0.0027
3	1.5	0.0302	0.0378181	0.007618	0.0003	0.0032
4	1.4775	0.0619	0.0701493	0.008249	0.0028	0.0004
5	1.47	0.0868	0.0798933	0.006907	0.0188	0.0153
6	1.445	0.1142	0.1085644	0.005636	0.0187	0.0138
7	1.37	0.1604	0.1623759	0.001976	0.0055	0.0075
8	0	0.3044	0.3042089	0.000191	0.0209	0.0026

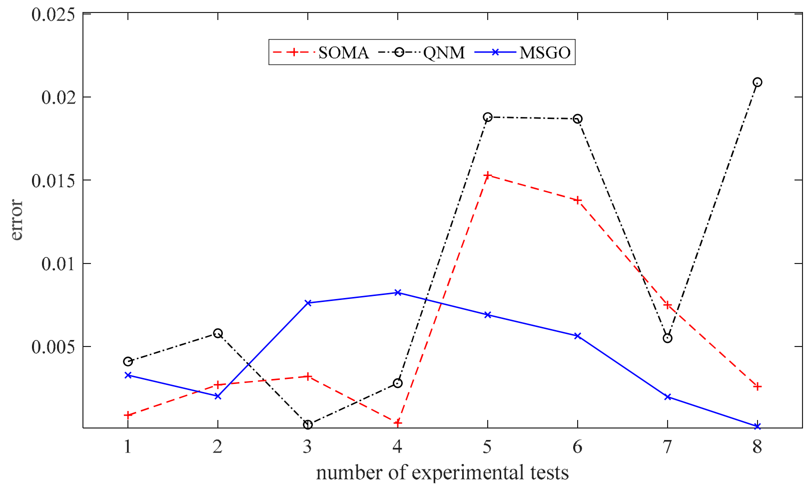

Figure 7. Estimated errors IAE.

Table 11. Statistical results for amorphous model.

	MSGO	SOMA	QNM
Total IAE	0.03587	0.04636	0.07690
RMSE	5.295×10^{-3}	7.952×10^{-3}	1.239×10^{-2}
SSE	2.243×10^{-4}	5.059×10^{-4}	1.228×10^{-3}
MAE	4.484×10^{-3}	5.796×10^{-3}	9.612×10^{-3}

4.2. Experimental Validation

The I–V and P–V characteristics of the TITAN-12-50 photovoltaic panel are implemented using the experimental test bench shown in Figure 8. The Parameter Specification of the TITAN-12-50 PV module is given in Table 12. To determine the various parameters of the photovoltaic generator, voltage and current measurements are required. These measurements are carried out using the LV25-P voltage sensor (Octapart, New York, NY, USA) and LA25-NP current sensor (Infineon, Munich, Germany). The solar sensor based on TLO82 is used to measure solar irradiation; meanwhile, the temperature is measured with an LM335 temperature sensor (ES Systems, Neo Psychico, Greece). The voltage and current are varied utilizing a variable resistor. The electronic oscilloscope scopiX, II (OX 7104) (TiePie, Sneek, The Netherlands) is used to display and record this variation.

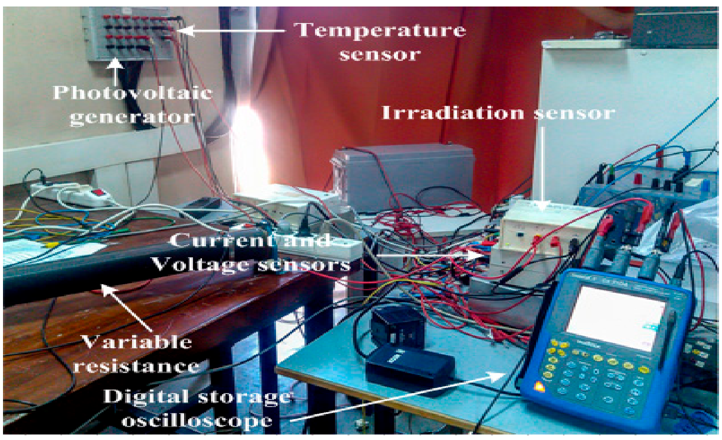

Figure 8. Experimental test bench.

Table 12. Parameter Specification of the TITAN-12-50 PV module.

Characteristics	Value
I_{sc} (A)	3.2
V_{0c} (V)	21
P_{mpp} (W)	50
I_{mpp} (A)	2.9
V_{mpp} (V)	17.2
Cells number	32

Several experiments are conducted in this study to evaluate the I–V and P–V characteristics of the developed models under various lighting and temperature conditions. Various environmental factors affect the performance of a PV generator under real-life conditions. Consequently, four different tests are performed, and their data are recorded and presented in Figures 9 and 10.

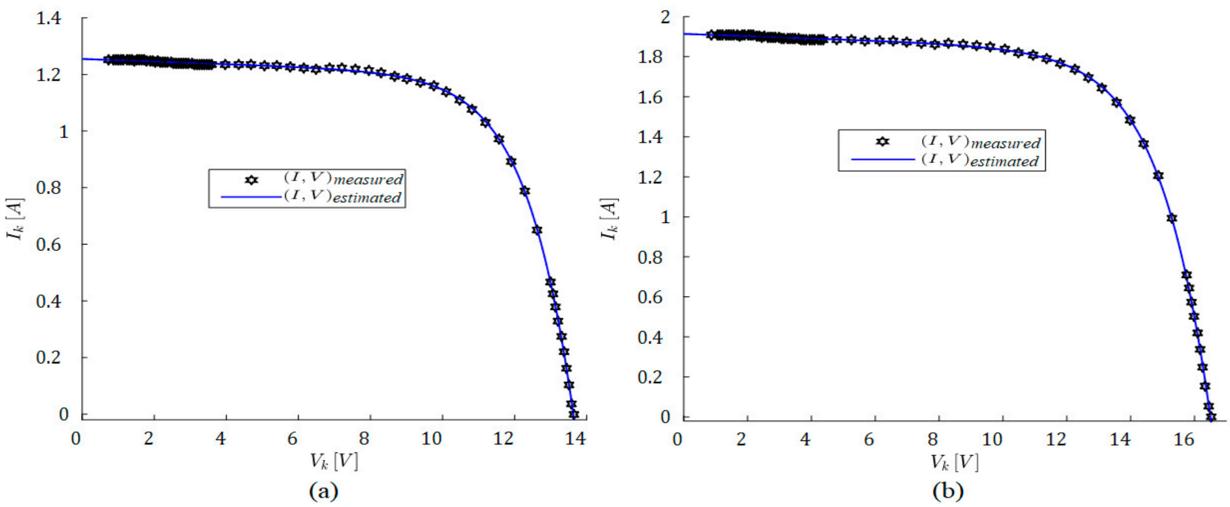

Figure 9. Comparison of I–V curves for TITAN-12-50 PV module using MSGO algorithm: (**a**) G = 360 W/m^2 and T = 18 °C; and (**b**) G = 556 W/m^2 and T = 20.5 °C.

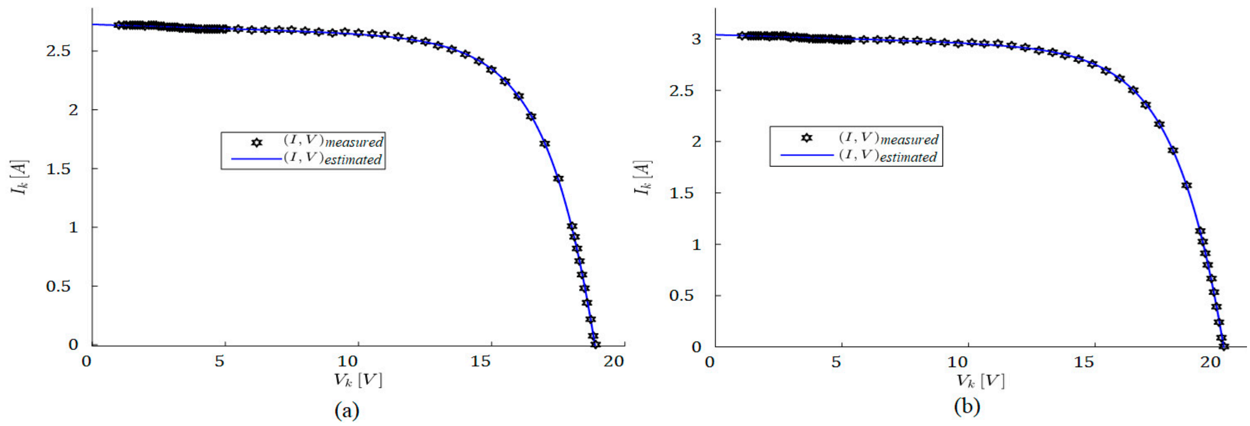

Figure 10. Comparison of I–V curves for TITAN-12-50 PV module using MSGO algorithm: (**a**) G = 810 W/m^2 and T = 22.60 °C; and (**b**) G = 900 W/m^2 and T = 23.80 °C.

According to the presented results in Figures 9 and 10, it can be noticed that the estimated current coincides with the measured current for the different cases of environmental factors.

This shows the effectiveness of the MSGO algorithm against changes in temperature and irradiation.

The convergence curves of various algorithms are illustrated in Figure 11. The average fitness functions ALO, WOA, VCS, GSA, SSA, and SCA are given in Ref. [40]. The MSGO results are presented in Figure 11 in black. In general, all algorithms exhibit an acceptable variation in the fitness function. The fastest convergence rate is seen in the MSGO results.

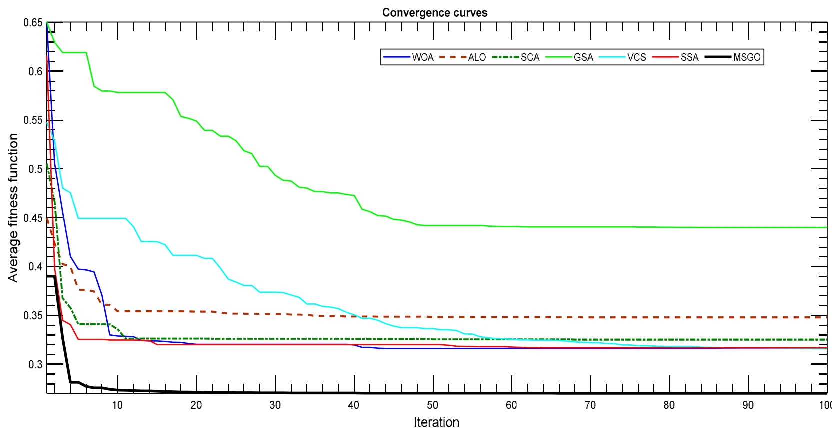

Figure 11. Average fitness functions.

All different parameters of the TITAN-12-50 solar panel extracted under G = 810 W/m^2 and T = 22.70 °C are illustrated in Table 13.

Table 13. Obtained RMSE values and estimated parameters of PV cells.

Parameters	I_{ph} (A)	R_s (Ω)	R_p (Ω)	α_1	α_2	I_{01} (μA)	I_{02} (μA)	RMS
MSGO	3.2810	0.3562	105.6204	1.4046	1.4046	4.48	4.48	1.3637×10^{-6}
SCA	2.74	0.169	72.000	1.456	1.200	9	9	1.3937×10^{-5}
ALO	2.733	0.489	50	1	1	0.6869	0.6786	1.5665×10^{-4}
GSA	2.716	0.818	140.659	1.013	1.058	0.6999	0.6405	4.8032×10^{-5}
VCS	2.734	0.333	70.189	1.003	1.002	0.6990	0.6993	1.6188×10^{-6}
WOA	2.75	0.351	90	1.60	1.48	7	7	3.6935×10^{-4}
SSA	2.722	0.174	98	1.2	1.3	7.8	7.8	1.5777×10^{-6}

Table 13 shows the extracted parameters of the TITAN-12-50 PV module at G = 810 W/m^2 and T = 22.70 °C. The MSGO parameter results are compared with previous results, given by Ref. [40], taking into account the same temperature and irradiation conditions. The proposed MSGO algorithm achieved the lowest RMSE value compared to all other algorithms by 1.3637×10^{-6}. After analyzing the data presented in Table 13, Figure 10, and Figure 11, it can be inferred that the MSGO algorithm exhibits several advantages, such as rapid convergence and minimal errors.

5. Discussion

The MSGO algorithm was developed to enhance the precision of solar cell parameter extraction. It was tested on monocrystalline, polycrystalline, and amorphous PV cells with the SDM and DDM to evaluate its performance. The MSGO algorithm was then compared to other techniques in the literature to determine its effectiveness. Results from statistical analysis and figures indicate that the MSGO algorithm is highly accurate and robust. Additionally, the results obtained from the MSGO algorithm are more promising than those of other previously proposed methods.

To further confirm the accuracy of the simulation model, experimental tests were conducted. The results of these tests indicate that the proposed MSGO algorithm is remarkably accurate, fast, and convergent, outperforming other similar algorithms proposed in the literature.

Author Contributions: All authors contributed to formulating the research idea, algorithm design, result analysis, writing, and reviewing the research. Conceptualization, H.K. and E.T.; data curation, E.T.; funding acquisition, E.T. and A.M.A.; investigation, M.J.; methodology, A.A. and A.M.A.; project administration, H.K.; resources, L.S.; software, T.I.A.; validation, A.A.; writing—original draft, H.K. and A.M.A.; writing—review and editing, T.I.A. All authors have read and agreed to the published version of the manuscript.

Funding: This work is funded by the Deanship of Scientific Research at Northern Border University under research group grant number (RG-NBU-2022-1215).

Institutional Review Board Statement: Not applicable.

Informed Consent Statement: Not applicable.

Data Availability Statement: Not applicable.

Acknowledgments: The authors extend their appreciation to the Deanship of Scientific Research at Northern Border University for funding this work through research group No. (RG-NBU-2022-1215). The authors gratefully thank the Prince Faisal bin Khalid bin Sultan Research Chair in Renewable Energy Studies and Applications (PFCRE) at Northern Border University for their support and assistance.

Conflicts of Interest: The authors declare no conflict of interest.

References

1. Ezzeddine, T. Reactive power analysis and frequency control of autonomous wind induction generator using particle swarm optimization and fuzzy logic. *Energy Explor. Exploit.* **2019**, *38*, 755–782. [CrossRef]
2. Touti, E.; Zayed, H.; Pusca, R.; Romary, R. Dynamic Stability Enhancement of a Hybrid Renewable Energy System in Stand-Alone Applications. *Computation* **2021**, *9*, 14. [CrossRef]
3. Kariem, H.; Touti, E.; Fetouh, T. The efficiency of PSO-based MPPT technique of an electric vehicle within the city. *Meas. Control.* **2020**, *53*, 461–473. [CrossRef]
4. Gul, M.; Kotak, Y.; Muneer, T. Review on recent trend of solar photovoltaic technology. *Energy Explor. Exploit.* **2016**, *34*, 485–526. [CrossRef]
5. Kihlström, V.; Elbe, J. Constructing Markets for Solar Energy—A Review of Literature about Market Barriers and Government Responses. *Sustainability* **2021**, *13*, 3273. [CrossRef]
6. Aminian, E.; Saffari, H. Experimental analysis of dropwise condensation heat transfer on a finned tube: Impact of pitch size. *Proc. Inst. Mech. Eng. Part A J. Power Energy* **2021**, *236*, 752–759. [CrossRef]
7. Belloni, M.; Conti, T.D.N. The Connection of Solar Generators to the Electricity Distribution Network as a Means of Mitigating Environmental Impacts by Dispensing the Banks of Accumulators. *Energy Power Eng.* **2019**, *11*, 392–397. [CrossRef]
8. Kumar, R.; Deshmukh, V.; Bharj, R.S. Performance enhancement of photovoltaic modules by nanofluid cooling: A comprehensive review. *Int. J. Energy Res.* **2020**, *44*, 6149–6169. [CrossRef]
9. Silva, P.R.; da Silva Jota, P.R.; Batista, A.P. PV Characterization System Outdoors—Case Study in Brazil. *J. Power Energy Eng.* **2017**, *05*, 119–132. [CrossRef]
10. Mokarram, M.; Mokarram, M.J.; Khosravi, M.R.; Saber, A.; Rahideh, A. Determination of the optimal location for constructing solar photovoltaic farms based on multi-criteria decision system and Dempster–Shafer theory. *Sci. Rep.* **2020**, *10*, 8200. [CrossRef]
11. Kraiem, H.; Aymen, F.; Yahya, L.; Triviño, A.; Alharthi, M.; Ghoneim, S.S.M. A Comparison between Particle Swarm and Grey Wolf Optimization Algorithms for Improving the Battery Autonomy in a Photovoltaic System. *Appl. Sci.* **2021**, *11*, 7732. [CrossRef]
12. Stutenbaeumer, U.; Mesfin, B. Equivalent model of monocrystalline, polycrystalline and amorphous silicon solar cells. *Renew. Energy* **1999**, *18*, 501–512. [CrossRef]
13. Anani, N.; Ibrahim, H.K. Adjusting the Single-Diode Model Parameters of a Photovoltaic Module with Irradiance and Temperature. *Energies* **2020**, *13*, 3226. [CrossRef]
14. Taherbaneh, M.; Rezaie, A.H.; Ghafoorifard, H.; Rahimi, K.; Menhaj, M.B.; Milimonfared, J.M. Evaluation of two-diode-model of a solar panel in a wide range of environmental conditions. *Int. J. Electron.* **2011**, *98*, 357–377. [CrossRef]
15. Qais, M.H.; Hasanien, H.M.; Alghuwainem, S.; Nouh, A.S. Coyote optimization algorithm for parameters extraction of three-diode photovoltaic models of photovoltaic modules. *Energy* **2019**, *187*, 116001. [CrossRef]
16. Premkumar, M.; Subramaniam, U.; Babu, T.S.; Elavarasan, R.M.; Mihet-Popa, L. Evaluation of Mathematical Model to Characterize the Performance of Conventional and Hybrid PV Array Topologies under Static and Dynamic Shading Patterns. *Energies* **2020**, *13*, 3216. [CrossRef]
17. Muhammadsharif, F.F.; Hashim, S.; Hameed, S.S.; Ghoshal, S.; Abdullah, I.K.; Macdonald, J.; Yahya, M.Y. Brent's algorithm based new computational approach for accurate determination of single-diode model parameters to simulate solar cells and modules. *Sol. Energy* **2019**, *193*, 782–798. [CrossRef]

18. Muhammadsharif, F.F.; Hashim, S. A Simple and Efficient Determination of the Ideality Factor of Solar Cells and Modules from the Knee Point of the Shunt Resistance Curve. *Arab. J. Sci. Eng.* **2023**, *48*, 8217–8225. [CrossRef]
19. DChan, D.S.H.; Phang, J.C.H. Analytical methods for the extraction of solar-cell single- and double-diode model parameters from I-V characteristics. *IEEE Trans. Electron Devices* **1987**, *34*, 286–293. [CrossRef]
20. Ibrahim, H.; Anani, N. Evaluation of Analytical Methods for Parameter Extraction of PV modules. *Energy Procedia* **2017**, *134*, 69–78. [CrossRef]
21. Oliva, D.; Cuevas, E.; Pajares, G.J.E. Parameter identification of solar cells using artificial bee colony optimization. *Energy* **2014**, *72*, 93–102. [CrossRef]
22. Narasimman, K.; Iniyan, S.; Goic, R. Experimental investigation of ridge concentrator PV-based solar water pumping system for small-scale applications. *Energy Sources Part A Recover. Util. Environ. Eff.* **2019**, *42*, 1844–1860. [CrossRef]
23. Fadlallah, S.O.; Serradj, D.E.B. Determination of the optimal solar photovoltaic (PV) system for Sudan. *Sol. Energy* **2020**, *208*, 800–813. [CrossRef]
24. Bastidas-Rodriguez, J.; Petrone, G.; Ramos-Paja, C.; Spagnuolo, G. A genetic algorithm for identifying the single diode model parameters of a photovoltaic panel. *Math. Comput. Simul.* **2017**, *131*, 38–54. [CrossRef]
25. Chen, X.; Xu, B.; Mei, C.; Ding, Y.; Li, K. Teaching–learning–based artificial bee colony for solar photovoltaic parameter estimation. *Appl. Energy* **2018**, *212*, 1578–1588. [CrossRef]
26. Yang, X.; Gong, W.; Wang, L. Comparative study on parameter extraction of photovoltaic models via differential evolution. *Energy Convers. Manag.* **2019**, *201*, 112113. [CrossRef]
27. Askarzadeh, A.; dos Santos Coelho, L. Determination of photovoltaic modules parameters at different operating conditions using a novel bird mating optimizer approach. *Energy Convers. Manag.* **2015**, *89*, 608–614. [CrossRef]
28. Kanimozhi, G.; Kumar, H. Modeling of solar cell under different conditions by Ant Lion Optimizer with LambertW function. *Appl. Soft Comput.* **2018**, *71*, 141–151. [CrossRef]
29. Subudhi, B.; Pradhan, R. Bacterial Foraging Optimization Approach to Parameter Extraction of a Photovoltaic Module. *IEEE Trans. Sustain. Energy* **2017**, *9*, 381–389. [CrossRef]
30. Saxena, A.; Sharma, A.; Shekhawat, S. Parameter extraction of solar cell using intelligent grey wolf optimizer. *Evol. Intell.* **2020**, *15*, 167–183. [CrossRef]
31. Elazab, O.S.; Hasanien, H.M.; Elgendy, M.A.; Abdeen, A.M. Parameters estimation of single- and multiple-diode photovoltaic model using whale optimisation algorithm. *IET Renew. Power Gener.* **2018**, *12*, 1755–1761. [CrossRef]
32. Kumar, C.; Raj, T.D.; Premkumar, M. A new stochastic slime mould optimization algorithm for the estimation of solar photovoltaic cell parameters. *Optik* **2020**, *223*, 165277. [CrossRef]
33. Ben Messaoud, R. Extraction of uncertain parameters of single and double diode model of a photovoltaic panel using Salp Swarm algorithm. *Measurement* **2019**, *154*, 107446. [CrossRef]
34. Naik, A.; Satapathy, S.C.; Abraham, A. Modified Social Group Optimization—A meta-heuristic algorithm to solve short-term hydrothermal scheduling. *Appl. Soft Comput.* **2020**, *95*, 106524. [CrossRef]
35. Hamid, N.F.A.; Rahim, N.A.; Selvaraj, J. Solar cell parameters identification using hybrid Nelder-Mead and modified particle swarm optimization. *J. Renew. Sustain. Energy* **2016**, *8*, 015502. [CrossRef]
36. Dkhichi, F.; Oukarfi, B.; Fakkar, A.; Belbounaguia, N. Parameter identification of solar cell model using Levenberg–Marquardt algorithm combined with simulated annealing. *Sol. Energy* **2014**, *110*, 781–788. [CrossRef]
37. Niu, Q.; Zhang, L.; Li, K. A biogeography-based optimization algorithm with mutation strategies for model parameter estimation of solar and fuel cells. *Energy Convers. Manag.* **2014**, *86*, 1173–1185. [CrossRef]
38. Gong, W.; Cai, Z. Parameter extraction of solar cell models using repaired adaptive differential evolution. *Sol. Energy* **2013**, *94*, 209–220. [CrossRef]
39. Askarzadeh, A.; Rezazadeh, A. Artificial bee swarm optimization algorithm for parameters identification of solar cell models. *Appl. Energy* **2013**, *102*, 943–949. [CrossRef]
40. Yuan, X.; He, Y.; Liu, L. Parameter extraction of solar cell models using chaotic asexual reproduction optimization. *Neural Comput. Appl.* **2014**, *26*, 1227–1239. [CrossRef]
41. Wang, Y.; Xi, J.; Han, N.; Xie, J. Modeling method research of flexible amorphous silicon solar cell. *Appl. Sol. Energy* **2015**, *51*, 41–46. [CrossRef]
42. Abbassi, R.; Abbassi, A.; Heidari, A.A.; Mirjalili, S. An efficient salp swarm-inspired algorithm for parameters identification of photovoltaic cell models. *Energy Convers. Manag.* **2018**, *179*, 362–372. [CrossRef]
43. Rodrigo, P.; Fernández, E.; Almonacid, F.; Pérez-Higueras, P. Models for the electrical characterization of high concentration photovoltaic cells and modules: A review. *Renew. Sustain. Energy Rev.* **2013**, *26*, 752–760. [CrossRef]
44. Bishop, J. Computer simulation of the effects of electrical mismatches in photovoltaic cell interconnection circuits. *Sol. Cells* **1988**, *25*, 73–89. [CrossRef]
45. Sulyok, G.; Summhammer, J. Extraction of a photovoltaic cell's double-diode model parameters from data sheet values. *Energy Sci. Eng.* **2018**, *6*, 424–436. [CrossRef]
46. Elazab, O.S.; Hasanien, H.M.; Alsaidan, I.; Abdelaziz, A.Y.; Muyeen, S.M. Parameter Estimation of Three Diode Photovoltaic Model Using Grasshopper Optimization Algorithm. *Energies* **2020**, *13*, 497. [CrossRef]

47. Satapathy, S.; Naik, A. Social group optimization (SGO): A new population evolutionary optimization technique. *Complex Intell. Syst.* **2016**, *2*, 173–203. [CrossRef]
48. Naik, A.; Satapathy, S.C.; Ashour, A.S.; Dey, N. Social group optimization for global optimization of multimodal functions and data clustering problems. *Neural Comput. Appl.* **2016**, *30*, 271–287. [CrossRef]